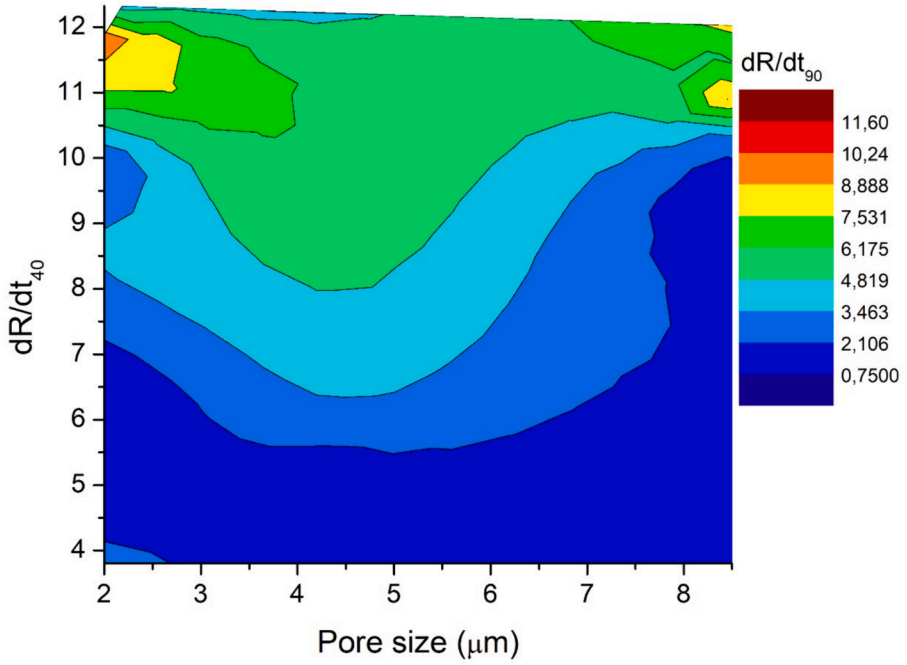

Fig. 12. dR/dt90 as a function of pore size and dR/dt40.

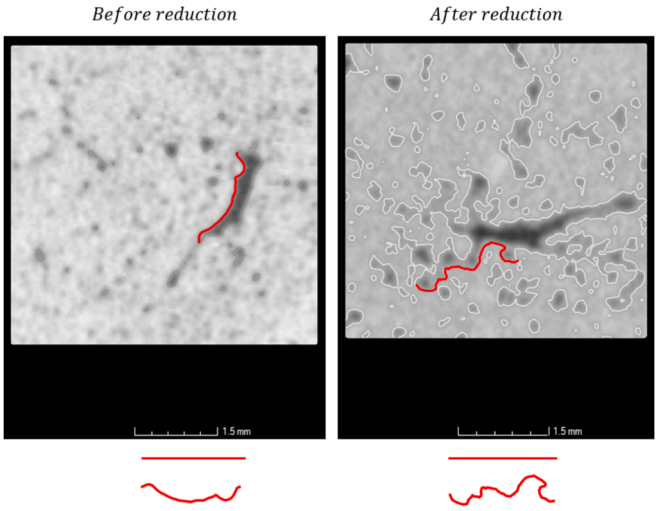

Fig. 13. Small pellet before reduction and after reduction at 1000 °C for 90 min.

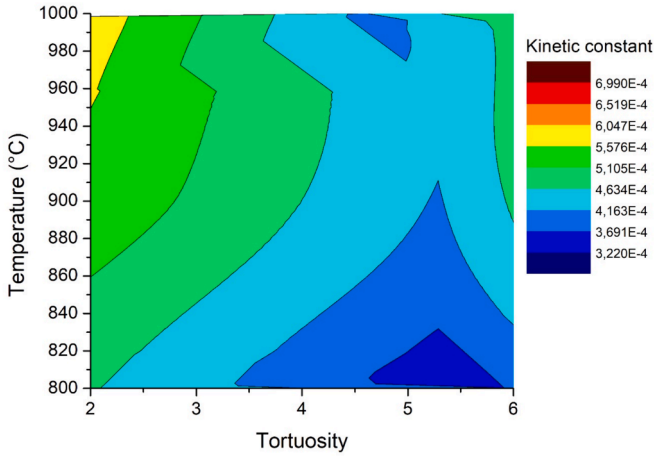

Fig. 14. Kinetic constant as a function of reduction temperature and pores tortuosity.

gas diffusion occurs very rapidly, resulting in significantly reduced reduction times. Therefore, the time required for reduction is shorter for low-density pellets, which in this specific scenario are also characterized by intermediate surface pore dimensions.

The contribution to entropy generation from mass transfer is another significant factor in the reduction process. Highly porous pellets can approach zero entropy generation due to enhanced gas penetration inside the pellets. However, entropy is never null because of the compositional gradient between the pellet surface and the yet-to-be-reduced core. Heat transfer has the most significant effect on entropy generation, followed by chemical reactions, while mass transfer has the smallest impact. During the initial stages of reduction, both chemical reactions and gas diffusion control the process, while in the later stages, the rate-limiting step becomes the interfacial chemical reactions. The calculation of the dR/dt40 index is typically used to assess the first (rapid) stage of reduction. This index is highly dependent on pellet density, as illustrated in Fig. 11.

Pellets with very small surface pores and a denser surface, typically seen in medium-sized pellets, develop a robust iron layer on the surface during reduction. This dense and hard iron layer has a significant adverse effect on the reduction rate. the development of a dense and hard iron layer during reduction has a significant adverse effect on the reduction rate of pellets with very small surface pores and a denser surface. Gas penetration through these hard iron layers can be enhanced at higher temperatures, but this can lead to softening of the pellets, reducing their porosity and affecting reduction rates. The final reduction stage of the overall process is typically assessed using the dR/dt90 index as depicted in Fig. 12.

As already observed, the pores aspect strongly varies during reduction.

As porosity increases, the dimensions of individual pores also increase, and the tortuosity of the pores varies, as illustrated in Fig. 13. Consequently, tortuosity tends to continuously change during the

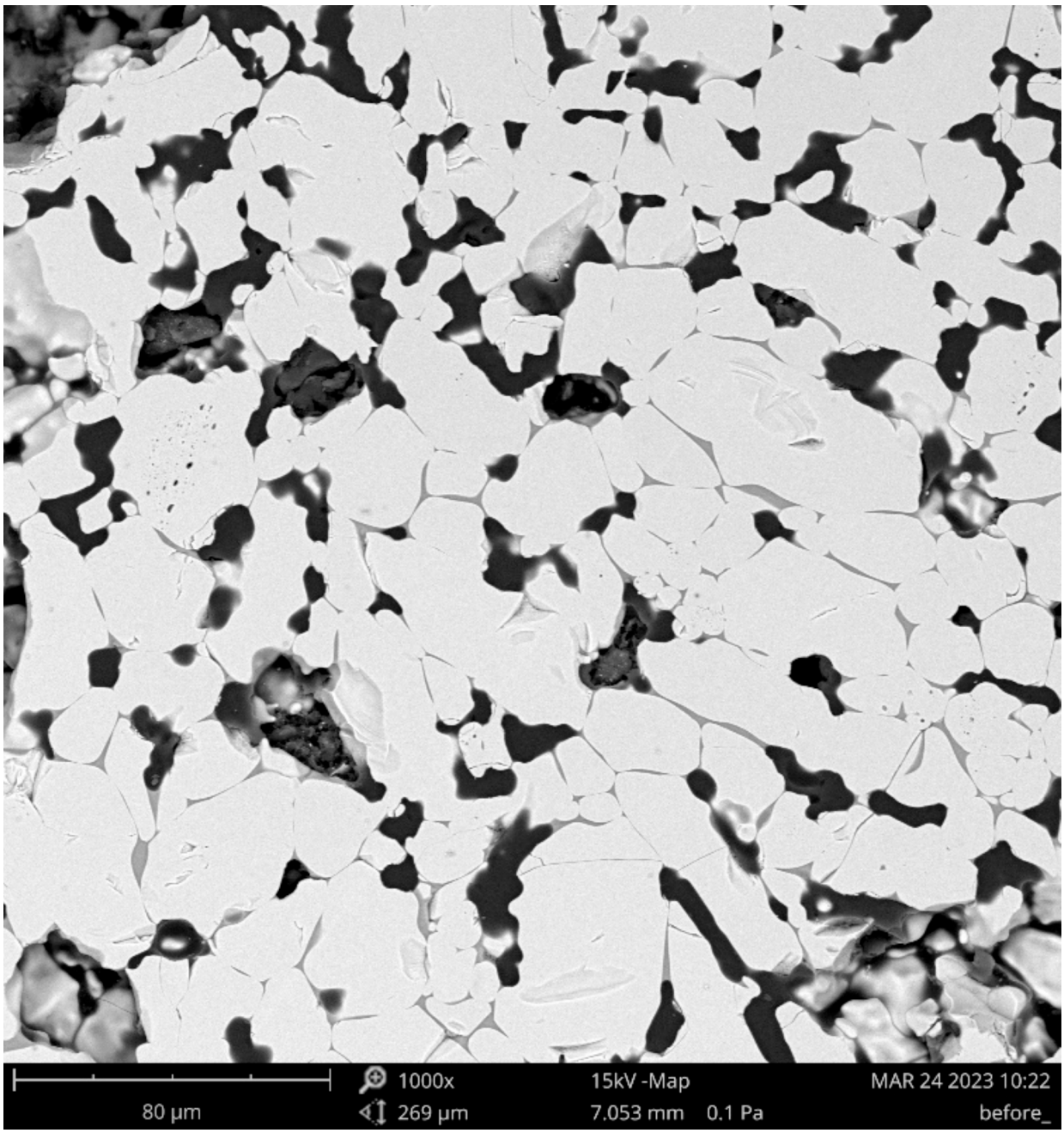

Fig. 15. SEM microstructure of the pellets before reduction.

reduction process. The initial value of tortuosity and its variation during reduction have a notable impact on pellet kinetics. The general behavior of reduction kinetics as a function of temperature and pore tortuosity is presented in Fig. 14.

Tortuosity delays the reduction process for a given temperature. As tortuosity increases, the turbulence of gas flowing within the pores also increases, leading to a decrease in the reduction rate. Under such conditions, the reduction rate tends to decrease. Considering the tortuosity factor within the pellets, The time required for reduction increases as pore tortuosity increases, porosity decreases (resulting in increased density), and pore dimensions decrease. These parameters significantly contribute to variations in entropy generated throughout all the reduction phases.

Entropy begins to increase in the initial stages of direct reduction due to heat transfer between the heated hydrogen and the pellet surface. Entropy continues to rise as porosity and the gas ratio decrease due to reduced exchange surfaces. Further increases in entropy generation occur as pore tortuosity increases (Sundberg, 2021). Tortuosity acts as an obstacle to gas flow and its ideal path within the pellet, thereby reducing overall gas diffusion and its reduction effect (Ali et al., 2022). Tortuosity has substantial implications for overall entropy behavior and energy input during the direct reduction process. Additionally, tortuosity has a greater impact as pellet diameter increases. As tortuosity increases, both entropy generation and energy consumption increase (Gautam and Cole, 2022; Singh et al., 2022), and entropy generation tends to exhibit a nonlinear behavior, particularly in the final stages of reduction when pellet tortuosity is highly pronounced. The microstructural analyses of the pellets evolution was performed through SEM and microanalyses (Fig. 15).

Based on our previous studies, we have found that the basicity index

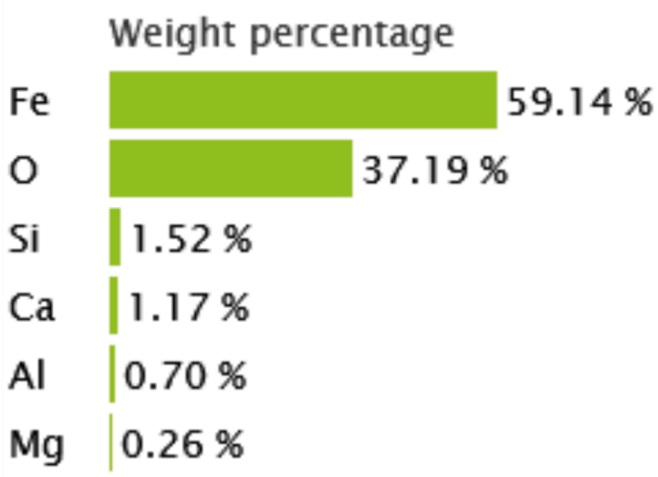

Fig. 15. (*continued*).

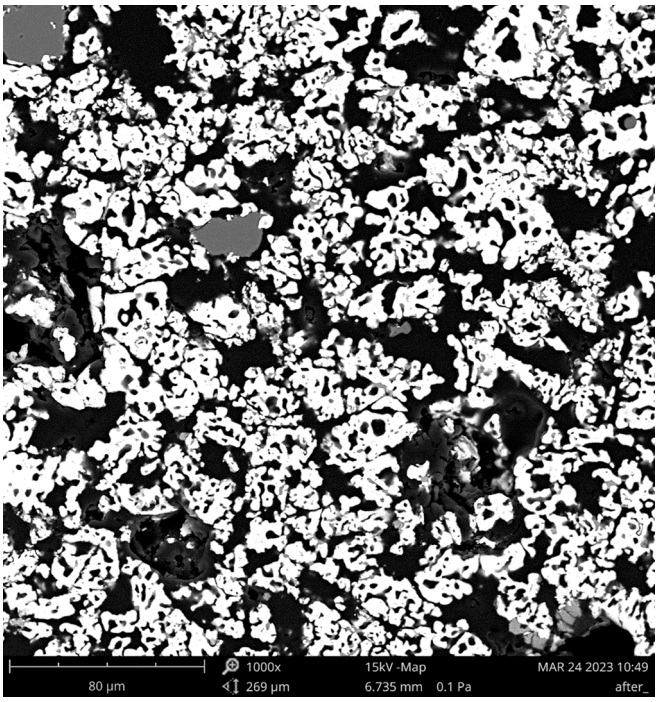

Fig. 16. SEM microstructure after reduction at 1000 °C for 30 min.

plays a crucial role in accelerating reduction reactions. However, the relationship between reduction behavior and the basicity index is complex. Experimental evidence has shown that reduction kinetics tend to increase as the basicity index varies from 0 to 1, but then it begins to decrease again as the basicity index increases. This suggests a parabolic relationship between the time required for reduction and the basicity index. Therefore, the reduction behavior of industrial pellets is closely tied to the quality of the raw material, which in turn influences the process and the quality of the final product for subsequent operations. Maintaining the basicity index at an appropriate level is essential for optimizing the pellet reduction process. This effect is more pronounced when there is a higher presence of CaO in the pellet composition. An excessive amount of CaO can make the produced pellets overly brittle, making them challenging to handle in subsequent processing operations. In our observations, hematite predominates in all regions, with localized occurrences of Ca-ferrite, particularly in the edge and outer

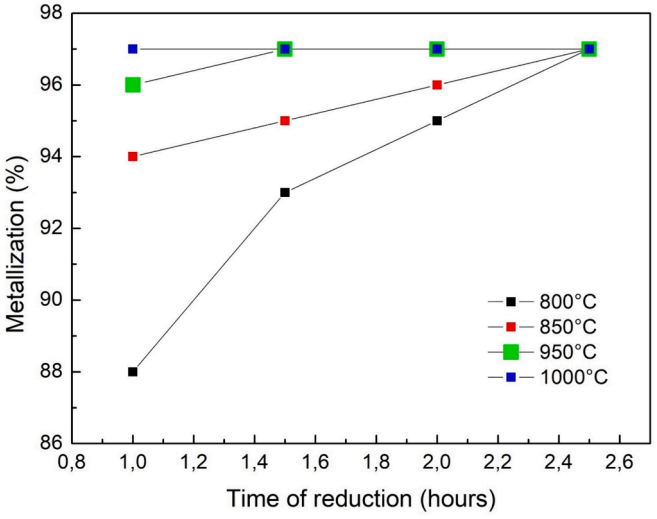

Fig. 17. Metallization degree as a function of temperature and time to reduction.

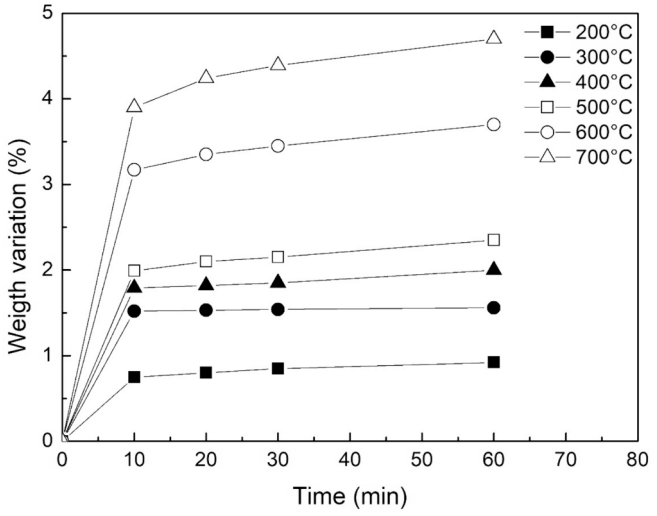

Fig. 18. Weight variation of the pellets as a function of temperature and pressure (reoxidation curves refer to the pellets with larger diameter).

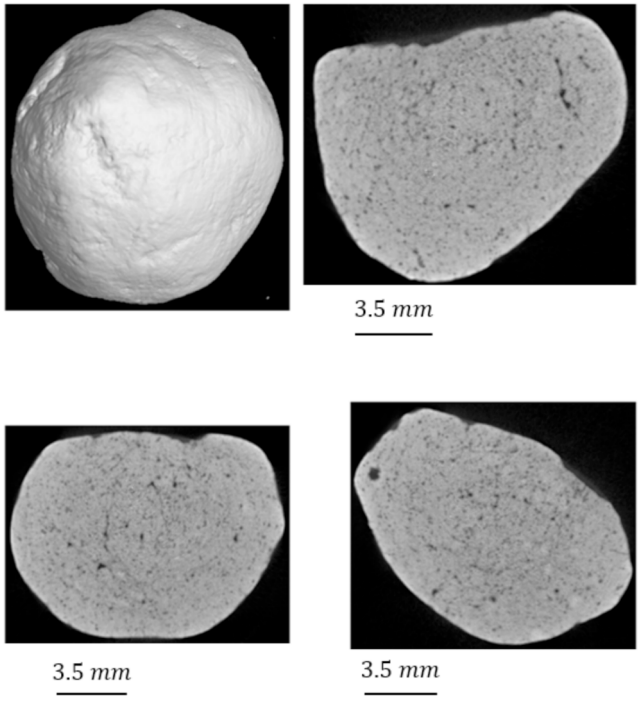

Fig. 19. Aspect of the pellets (medium size) after reoxidation at 700 °C for 60 min.

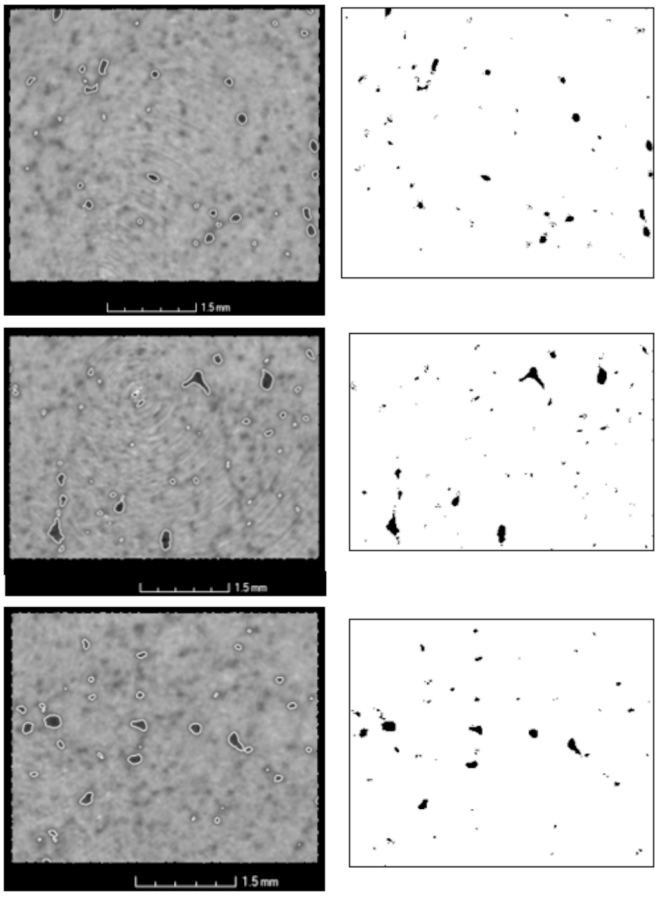

Fig. 20. Porosity measurement of the reoxidized pellet.

mantle regions. We have also noted intergranular porosity and medium-sized pores, likely originating from certain inputs. Calcium silicate permeates the gaps between hematite particles.

Hematite is the dominant mineral observed in all regions, with localized occurrences of Ca-ferrite, particularly in the edge and outer mantle regions. Intergranular porosity and medium-sized pores are also present, likely originating from certain inputs or processes. Calcium silicate is found permeating the spaces between hematite particles. After completed metallization the aspect of the pellets microstructure is shown in Fig. 16.

In all regions, it is observed the predominance of metallic Fe. Despite the substantial transformation, it is still possible to identify the contours of the previous oxide phase. The reduced pellet exhibits high porosity, allowing us to distinguish intergranular porosity, which remains from the oxide particles, and intragranular porosity, generated during the transformation of metallic Fe oxide. Furthermore, various tests were performed to assess the metallization and reducibility of numerous pellets, each weighing hundreds of grams. The rate of metallization increases as the reactor temperature rises, as illustrated in Fig. 17.

When considering the time required for reduction, it becomes evident that the primary influencing factor is the pellet diameter, followed by pellet density, both of which have a direct correlation. Gas temperature and pore size exhibit an inverse correlation with the reduction time. Interestingly, pores' tortuosity appears to have a lesser impact, showing a direct correlation with the reduction time.

The effect of pellet size on the reduction process is influenced by pellet density. For high-density pellets, the impact of pellet diameter decreases, while the opposite is observed for larger particles, where density has a reduced effect (Scharm et al., 2022). Consequently, the time required to achieve reduction is primarily dependent on the size of surface pores. Larger pores lead to faster pellet reduction. However, this relationship is also influenced by pellet density, as an increase in pellet density results in a longer time to reduction. Additionally, when considering individual pores, pore tortuosity plays a role in the time to reduction. At the same pore size, an increase in tortuosity leads to a longer time to reduction. In the case of high-density pellets, reduction reactions occur in a stepwise manner and can be modeled through a shrinking core description. This leads to longer reduction times, which are directly proportional to pellet size. Conversely, low-density pellets allow for rapid gas diffusion, resulting in significantly shorter reduction times. Thus, the time required for reduction is shorter for low-density pellets, particularly when they also have intermediate-sized surface pores (Pal et al., 2017; Nguyen et al., 2021). The tortuosity of pores inside the pellets further influences the time to reduction, with increased tortuosity, decreased porosity (increased density), and smaller pore dimensions all leading to longer reduction times.

The behavior of pellet reduction in hydrogen direct reduction is influenced by a hierarchy of phenomena that span from macroscopic scales to atomic ones. These phenomena are contingent on kinetic behavior and encompass heat and mass transfer, involving catalytic processes, diffusion, dissociation, and charge transfer. The intricate nonlinear interactions between these phenomena necessitate the use of diverse characterization and modeling tools for comprehensive understanding. The effects of reduction degree, temperature, and atmosphere on the swelling behavior of pellets have been studied thoroughly under typical hydrogen-based shaft furnaces. Computational analysis of hydrogen reduction of iron oxide pellets in a shaft furnace process has also been conducted. The model relies on a detailed description of the main physical–chemical and thermal phenomena, using a multi-scale approach. The calculated results reveal the detailed behavior of the reduction process, which is likely to reduce CO2 emissions from the steel industry.

The behavior of pellet reduction is influenced by macroscopic transport and diffusion of gases, which play varying roles at different scales within the process. These roles are intimately linked to the microstructure and chemical-physical properties of the pellets. At the

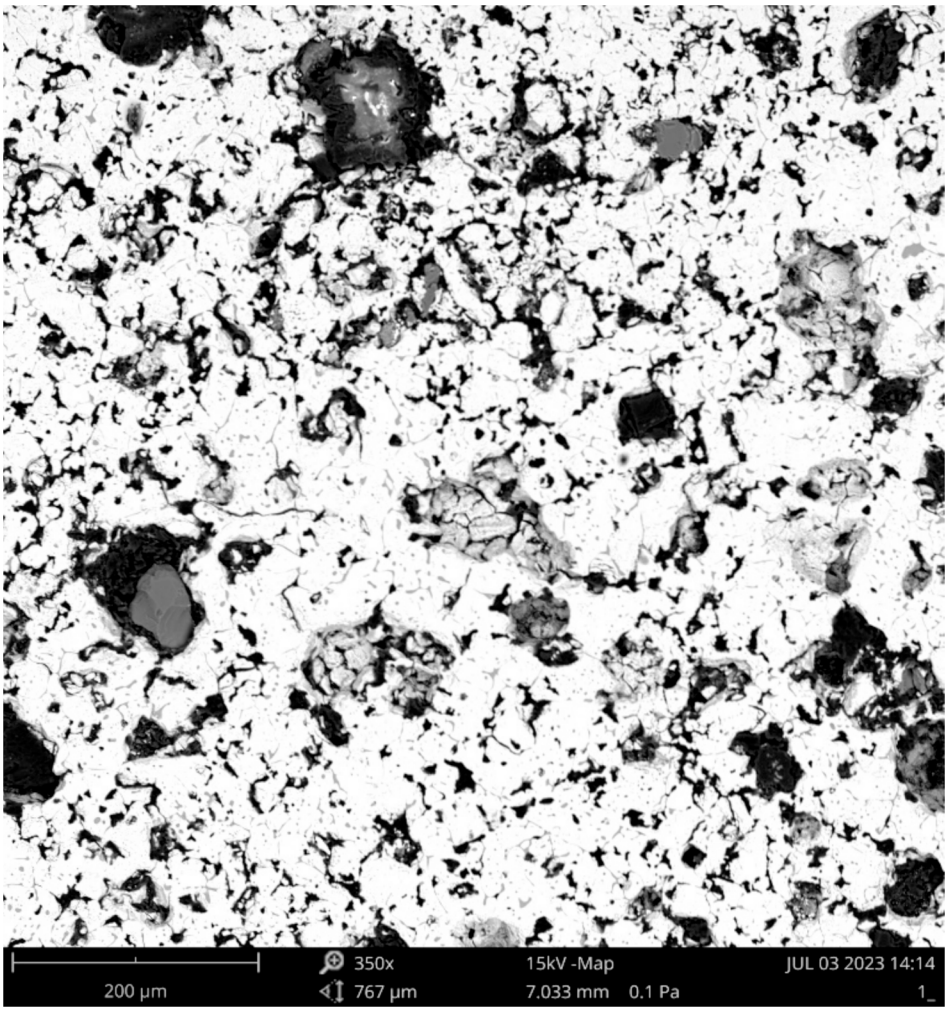

Fig. 21. SEM microstructure of the pellet after reoxidation.

microscale, process kinetics are shaped by phenomena occurring at both micro and atomic scales due to the transformations involving different oxides, crystal defects, and local compositions. Several macroscopic studies exist on the reduction of iron oxide exposed to different gas mixtures, and these studies play a critical role in the reduction process itself (Chai et al., 2022; Fan et al., 2021; Chai et al., 2022). The reduction swelling process of pellets prepared from the Bayan Obo iron ore concentrate has been explored based on the iron oxide reduction. The reducing reactions of different composite pellets were mainly controlled by gasification diffusion. The reduction rates can be described by the kinetic analysis. The effect of iron ore pellet size on metallurgical properties has also been studied, and it was found that the size distribution is important for the permeability of the ore burden layers in the furnace. The swelling of pellets characterizes the vulnerability to change in volume during reduction and is tested to ensure that the volume increase during reduction does not exceed a set maximum.

The reduction process of iron ore pellets is influenced by various factors, including processing conditions, pellet composition, density, porosity, and size. Tortuosity plays a significant role in reduction kinetics, as highly tortuous pellets exhibit reduced reaction kinetics, both temporally and spatially. As tortuosity increases, the kinetic constants decrease, as fewer hydrogen atoms interact with the material bulk under similar conditions of pressure, temperature, and mass transfer. Precisely, highly tortuous pellets exhibit reduced reaction kinetics, both temporally and spatially. Consequently, the degree of metallization of pellets is dependent on temperature, followed by tortuosity, gas temperature, pellet diameter, and, finally, density and pore size. The most influential parameter governing metallization behavior is the reduction temperature. The degree of metallization is dependent on temperature, followed by tortuosity, gas temperature, pellet diameter, and, finally, density and pore size (Iljana et al., 2022; Sadeghi et al., 2024; Cavaliere et al., 2024; Cavaliere et al., 2024).

Subsequent to complete metallization, the pellets underwent reheating at various temperatures to assess their reoxidation behavior, and the results are depicted in Fig. 18.

Oxidation initially occurs at low temperatures through the reaction of metallic iron with humidity in the air:

$$2Fe + H_2O + 3O \leftrightarrow 2FeOOH$$

These reactions are very exothermic and release an amount of heat that provides enough energy to enable the other oxidation reactions:

$$3Fe + 2O_2 \leftrightarrow Fe_3O_4$$

$$2Fe_3O_4 + \frac{1}{2}O_2 \leftrightarrow 2Fe_2O_3$$

$$Fe + \frac{1}{2}O_2 \leftrightarrow FeO$$

The last reaction takes place above 570 °C.

The oxidation process of iron sponge is characterized by three distinct stages, each with a different rate of oxidation. The first stage is the rapid initial stage, where the oxidation rate is high, and chemical

reactions at the interfaces play a dominant role. The second stage is the intermediate stage, where the oxidation rate gradually decreases, and diffusion in the solid state becomes the controlling mechanism. The final stage is marked by a low and almost constant rate of oxidation, where solid-state diffusion with the formation of cavities at the interfaces between the oxide film and the metallic iron grains is the predominant mechanism. The observed behavior is influenced by several factors, including the rapid reduction in porosity during oxidation, which limits the diffusion of the oxidizing gas and the reactivity of the particle surfaces. As a result, the rate of oxidation decreases, and non-porous oxide layers block further oxidation. This complex interplay of mechanisms leads to the observed stages in the oxidation process. The oxidation process is exothermic, leading to a significant increase in the temperature of the iron sponge as heat is released. The behavior of the oxidation process is influenced by several factors, including processing conditions, porosity, and the reactivity of the particle surfaces.

The microtomography aspect of the medium size pellet after reoxidation at 700 °C for 60 min is shown in Fig. 19.

The porosity aspect after reoxidation is shown in Fig. 20.

The SEM microstructure and the compositional map of the medium size pellets after reoxidation at 700 °C for 60 min is shown in Fig. 21.

The analysis of the reoxidized pellets reveals a complex transformation process. Metallic iron (Fe) dominates in the reoxidized pellets, indicating that a substantial portion of the initially reduced iron remains in its metallic state after reoxidation. Minor phases such as silicates and Ca-ferrites are also present, suggesting the existence of impurities or secondary compounds. The pellets exhibit a zoned structure, with the core primarily transforming into hematite, an iron oxide. At the outer mantle, a narrow magnetite-wustite transition zone is observed, mainly in the region containing metallic iron. Importantly, the Fe-metallic phase remains preserved in the core. Additionally, some regions show a coexistence of magnetite and wustite without clear boundaries. This complex behavior underscores the intricate nature of iron oxide phase transformations during reoxidation, providing valuable insights for understanding the properties and applications of these materials.

4. Conclusions

In view of the extensive research performed in this study, many important conclusions can be drawn. The careful microtomographic studies performed on individual pellets, both before and after direct hydrogen reduction, have provided a comprehensive mapping of the porosity evolution in these materials. It is evident that porosity, pore size, and pore tortuosity vary as a function of specific processing parameters, especially with temperature variations and a gas pressure of 8 bar. These variations in porosity properties have profound effects on the kinetics of the reduction process, as the rate of porosity change is strongly influenced by temperature conditions. Consequently, this leads to variations in diffusion dynamics and gas–solid interactions throughout the reduction process. Multi-pellet reduction experiments have shown that satisfactory metallization occurs at temperatures above 850 °C. Overall, these comprehensive findings contribute to a deeper understanding of the behavior of iron ore pellets during the production and reduction processes and ultimately provide information for strategies to optimize their performance in industrial applications.

CRediT authorship contribution statement

Pasquale Cavaliere: Conceptualization, Data curation, Funding acquisition, Investigation, Methodology, Project administration, Supervision, Validation, Writing – original draft, Writing – review & editing. **Behzad Sadeghi:** Investigation. **Leandro Dijon:** Resources. **Aleksandra Laska:** Data curation, Formal analysis, Investigation. **Damian Koszelow:** Data curation, Formal analysis, Investigation.

Declaration of competing interest

The authors declare that they have no known competing financial interests or personal relationships that could have appeared to influence the work reported in this paper.

Data availability

Data will be made available on request.

Acknowledgments

Authors would like to thank the Italian Ministry for University and Research (MUR) for the fundings provided under the Grant “Low environmental impact fuels for metallurgical industries- 2022P3PJXN”.

Appendix A. Supplementary data

Supplementary data to this article can be found online at https://doi.org/10.1016/j.mineng.2024.108746.

References

Ali, M.L., Fradet, Q., Riedel, U., 2022. Kinetic Mechanism development for the direct reduction of single hematite pellets in H_2/CO atmospheres. Steel Res. Int. 93 (12), 2200043. https://doi.org/10.1002/srin.202200043.

Anameric, B., Kawatra, K., 2007. Properties and features of direct reduced iron. Miner. Proc. Extract. Metall. Rev. 28 (1), 59–116. https://doi.org/10.1080/08827500600835576.

Augusto, K.S., Alves, H.D.L., Mauricio, M.H.d.P., Paciornik, S. 3D characterization of iron ore pellets by X-ray microCT. *Image Analysis & Stereology,* 14th International Congress for Stereology and Image Analysis Liège, (2015) July 7-10.

Ba, Y., Mianroodi, J.R., Ma, Y., Silva, A.K.D., Svendsen, B., Raabe, D., 2022. Chemo-mechanical phase-field modeling of iron oxide reduction with hydrogen. Acta Mater. 231, 117899 https://doi.org/10.1016/j.actamat.2022.117899.

Bersenev, I.S., Vokhmyakova, I.S., Borodin, A.V., Pigarev, S.P., Sivkov, O.G., Zagainov, S. A., 2022. Structure and metallurgical properties formation of semireduced pellets. Steel Transl. 52, 331–336. https://doi.org/10.3103/S0967091222030160.

Bezerra, E.T.V., Augusto, K.S., Paciornik, S., 2020. Discrimination of pores and cracks in iron ore pellets using deep learning neural networks. REM, Int. Eng. J. 73 (2) https://doi.org/10.1590/0370-44672019730119.

Biswas, C., Swarnakar, A., Majumder, A., 2023. Utilization of micro-fines in sinter making and its implications on bed permeability and sinter quality. Ironmak. Steelmak. https://doi.org/10.1080/03019233.2022.2163532.

Cavaliere, P., Perrone, A., Marsano, D., 2023. Critical analysis of variable atmosphere gaseous reduction of iron oxides pellets. Ironmak. Steelmak. https://doi.org/10.1080/03019233.2023.2194732.

Cavaliere, P., Perrone, A., Marsano, D., Primavera, V., 2023. Hydrogen-based direct reduction of iron oxides pellets modeling. Steel Res. Int. 94 (6), 2200791. https://doi.org/10.1002/srin.202200791.

Cavaliere, P., Perrone, A., Marsano, D., 2023. Effect of reducing atmosphere on the direct reduction of iron oxides pellets. Powder Technol. 426, 118650 https://doi.org/10.1016/j.powtec.2023.118650.

Cavaliere, P., Perrone, A., Dijon, L., Laska, A., Koszelow, D., 2024. Direct reduction of pellets through hydrogen: Experimental and model behaviour. Int. J. Hydrogen Energy 49C, 1444–1460. https://doi.org/10.1016/j.ijhydene.2023.11.040.

Cavaliere, P., Dijon, L., Laska, A., Koszelow, D., 2024. Hydrogen direct reduction and reoxidation behaviour of high-grade pellets. Int. J. Hydrogen Energy 49C, 1235–1254. https://doi.org/10.1016/j.ijhydene.2023.08.254.

Cavaliere, P. (2019). Blast Furnace: Most Efficient Technologies for Greenhouse Emissions Abatement. In: Clean Ironmaking and Steelmaking Processes. Springer, Cham. 10.1007/978-3-030-21209-4_4.

Cavaliere, P. (2019). Direct Reduced Iron: Most Efficient Technologies for Greenhouse Emissions Abatement. In: Clean Ironmaking and Steelmaking Processes. Springer, Cham. 10.1007/978-3-030-21209-4_8.

Cavaliere, P. (2019). Sintering: Most Efficient Technologies for Greenhouse Emissions Abatement. In: Clean Ironmaking and Steelmaking Processes. Springer, Cham. 10.1007/978-3-030-21209-4_3.

Chai, Y., Fan, Y., Gao, X., Luo, G.P., Wang, Y.-C., An, S., Liu, J., 2022. Effect of basicity on the reduction swelling performance of pellets prepared from Bayan obo iron ore concentrate based on microscopic characterization. Crystals.

Chai, Y., Fan, Y., Li, Z., Wu, J., Zhang, Y., Wang, Y.-C., Luo, G.P., An, S., 2022. Kinetics of reduction in stages of pellets prepared from the bayan obo iron ore concentrate. ACS Omega 7, 7759–7768.

El-Zoka, A.A., Stephenson, L.T., Kim, S.-H., Gault, B., Raabe, D., 2023. The fate of water in hydrogen-based iron oxide reduction. Adv. Sci. https://doi.org/10.1002/advs.202300626.

Fan, Y., Zhang, Y., Li, Z., Chai, Y., Wang, Y.-C., Luo, G.P., An, S., 2021. Mechanism on reduction swelling of pellets prepared from Bayan Obo iron ore concentrate. Ironmak. Steelmak. 48, 1158–1168.

Gautam, S., Cole, D.R., 2022. Effects of pore connectivity and tortuosity on the dynamics of fluids confined in sub-nanometer pores. PCCP 24, 11836–11847. https://doi.org/10.1039/D1CP04955K.

Ghadi, A.Z., Valipour, M.S., Biglari, M., 2016. Mathematical modelling of wustite pellet reduction: grain model in comparison with USCM. Ironmak. Steelmak. 43 (6), 418–425. https://doi.org/10.1080/03019233.2015.1135578.

Ghadi, A.Z., Radfar, N., Valipour, M.S., Sohn, H.Y., 2023. A review on the modeling of direct reduction of iron oxides in gas-based shaft furnaces. Steel Res. Int. 94 (6), 2200742. https://doi.org/10.1002/srin.202200742.

Hamadeh, H., Mirgaux, O., Patisson, F., 2018. Detailed modeling of the direct reduction of iron ore in a shaft furnace. Materials 11 (10), 1865. https://doi.org/10.3390/ma11101865.

Huang, Z., Yi, L., Jiang, T., 2012. Mechanisms of strength decrease in the initial reduction of iron ore oxide pellets. Powder Technol. 221, 284–291. https://doi.org/10.1016/j.powtec.2012.01.013.

Ignacio, I.R., Brooks, G., Pownceby, M.I., Rhamdhani, M.A., Rankin, W.J. 2022. Porosity in Iron Ore Sintering, AISTech 2022 — Proceedings of the Iron & Steel Technology Conference 16–18 May 2022, Pittsburgh, Pa., USA. 10.33313/386/215.

Iljana, M., Paananen, T., Mattila, O., Kondrakov, M., Fabritius, T., 2022. Effect of iron ore pellet size on metallurgical properties. Metals 12 (2), 302. https://doi.org/10.3390/met12020302.

Ju, J., Li, Q., Xing, X.D., Jiang, X., Zhao, G., Lu, F., 2023. Effect of high basicity on compressive strength and microstructure of iron ore pellets containing TiO_2. Metall. Res. Technol. 120 (3), 306. https://doi.org/10.1051/metal/2023032.

Kim, T., Sohn, I.l., 2023. Effects of K_2CO_3 addition on the physicochemical properties of goethite composite pellets with different basicities (CaO/SiO2). J. Mater. Res. Technol. 25, 4595–4608. https://doi.org/10.1016/j.jmrt.2023.06.247.

Korobeinikov, Y., Meshram, A., Harris, C., Kovtun, O., Govro, J., O'Malley, R.J., Volkova, O., Sridhar, S., 2023. Reduction of iron ore pellets using different gas mixtures and temperatures. Steel Res. Int. https://doi.org/10.1002/srin.202300066.

Lei Jie, Zhang Chen, An Jingshu, Kong Yu-qi, he shengping, Long Hongming, Wu Ting, Mechanism Study on Gas-Based Reduction Swelling Behavior of Ultra-High Grade Pellets. Available at SSRN: https://ssrn.com/abstract=4475187 or 10.2139/ssrn.4475187.

Li, J., Liang, Z., Yi, L., Huang, B., Chen, J., Han, H., Huang, Z., 2021. Novel insights into the reoxidation of direct reduced iron (DRI) during ball-mill treatment: A combined experimental and computational study. Appl. Surf. Sci. 552, 149485 https://doi.org/10.1016/j.apsusc.2021.149485.

Li, Z., Qi, Z., Zhang, L., Guo, M., Liang, D., Dong, Q., 2023. Numerical simulation of H_2-intensive shaft furnace direct reduction process. J. Clean. Prod. 409, 137059 https://doi.org/10.1016/j.jclepro.2023.137059.

Ljung, Anna-Lena. "Modeling drying of iron ore pellets." PhD diss., Luleå tekniska universitet, 2010.

Lyu, B., Wang, G., Xie, S., 2023. Effect of hydrogen-rich atmosphere on the reduction behavior and kinetics of iron-ore pellets under non-isothermal conditions. JOM 75, 1540–1550. https://doi.org/10.1007/s11837-022-05693-3.

Ma, K., Deng, J., Wang, G., Zhou, Q.i., Jian, Xu., 2021. Utilization and impacts of hydrogen in the ironmaking processes: A review from lab-scale basics to industrial practices. Int. J. Hydrogen Energy 46 (52), 26646–26664. https://doi.org/10.1016/j.ijhydene.2021.05.095.

Man, Y., Feng, J., 2016. Effect of gas composition on reduction behavior in red mud and iron ore pellets. Powder Technol. 301, 674–678. https://doi.org/10.1016/j.powtec.2016.06.013.

Meshram, A., Govro, J., OMalley, R.J., Sridhar, S., Korobeinikov, Y., 2022. Modeling isothermal reduction of iron ore pellet using finite element analysis method. Exp. Validat. Met. 12 (12), 2026. https://doi.org/10.3390/met12122026.

Metolina, P., de Andrade, R.S., Ramos, B., Guardani, R., 2023. Hydrogen direct reduction ironmaking process for zero CO_2 emission: A study on the effect of particle properties changes during the multiple non-catalytic gas-solid reactions. Miner. Eng. 201, 108188 https://doi.org/10.1016/j.mineng.2023.108188.

Mishra, S., 2020. Review on reduction kinetics of iron ore-coal composite pellet in alternative and sustainable ironmaking. J. Sustain. Metall. 6, 541–556. https://doi.org/10.1007/s40831-020-00299-y.

Mohammad, S., Patra, S., Harichandan, B., 2023. Reductants in iron ore sintering: A critical review. Fuel 332 (2), 126194. https://doi.org/10.1016/j.fuel.2022.126194.

Nguyen, C.-S., Nguyen, T.-H., Nguyen, S.-L., Bui, A.-H., 2021. Study on the reducibility of iron ore pellets at high temperature. Viet. J. Sci. Technol. Eng. 63 (4), 3–7. https://doi.org/10.31276/VJSTE.63(4).03-07.

Nie, H., Qi, B., Li, Y., Qiu, D., Wei, H., Hammam, A., Ahmed, A., Yaowei, Yu., 2023. Structure analysis of pellets with different reduction degrees using X-ray micro-computed tomography. Steel Res. Int. 94 (1), 2200241. https://doi.org/10.1002/srin.202200241.

Nurdiawati, A., Zaini, I.N., Wei, W., Gyllenram, R., Yang, W., Samuelsson, P., 2023. Towards fossil-free steel: Life cycle assessment of biosyngas-based direct reduced iron (DRI) production process. J. Clean. Prod. 393, 136262 https://doi.org/10.1016/j.jclepro.2023.136262.

Pal, J., Ghoari, S., Ammasi, A., Hota, S.K., Koranne, V.M., Venugopalan, T., 2017. Improving reducibility of iron ore pellets by optimization of physical parameters. J. Min. Metall. Sect. B-Metall. 53 (1), 37–46. https://doi.org/10.2298/JMMB151206014P.

Pfeiffer, A., Ernst, D., Zheng, H., Wimmer, G., Schenk, J., 2023. The behavior of direct reduced iron in the electric arc furnace hotspot. Metals 13 (5), 978. https://doi.org/10.3390/met13050978.

Rao, N.D., Chakraborty, D.P., Vishal Shukla, Neeraj Kumar. 2023. Iron ore beneficiation: an overview, Mineral Processing-Beneficiation Operations and Process Optimization Through Modeling pp. 55-77. 10.1016/B978-0-12-823149-4.00003-X.

Reddy, A.L.S.B., Sahoo, S.K., Kumar, M., 2023. Studies on characterization of properties of low-grade hematite iron ores and their fired pellets. Ironmak. Steelmak. https://doi.org/10.1080/03019233.2023.2180930.

Rukini, A., Rhamdhani, M.A., Brooks, G.A., 2022. Metals Production and metal oxides reduction using hydrogen: A review. J. Sustain. Metall. 8, 1–24. https://doi.org/10.1007/s40831-021-00486-5.

Sadeghi, B., Cavaliere, P., Bayat, M., Esfahani, N.E., Laska, A., Koszelow, D., 2024. Experimental study and numerical simulation on porosity dependent direct reducibility of high-grade iron oxide pellets in hydrogen. Int. J. Hydrogen Energy 69, 586–607. https://doi.org/10.1016/j.ijhydene.2024.05.050.

Scharm, C., Küster, F., Laabs, M., Huang, Q., Volkova, O., Reinmöller, M., Guhl, S., Meyer, B., 2022. Direct reduction of iron ore pellets by H_2 and CO: In-situ investigation of the structural transformation and reduction progression caused by atmosphere and temperature. Miner. Eng. 180, 107459 https://doi.org/10.1016/j.mineng.2022.107459.

Shen, Z., Sun, S., Jianliang, Xu., Liang, Q., Liu, H., 2023. Experimental and modeling study on reduction and heat transfer characteristics of single iron ore pellet in H_2/CO atmospheres. ISIJ Int. 63 (1), 42–53. https://doi.org/10.2355/isijinternational.ISIJINT-2022-280.

Singh, A.K., Kumar, A., Kumar, S., Mishra, B., Biswajit, Dishwar, R.K., Mandal, A.K., Rao, L.S., Sinha, O.P., 2022. Direct reduction of fluxed iron ore pellets made from coarse iron ore particles. Can. Met. Quat. 61 (4), 475–482. https://doi.org/10.1080/00084433.2022.2045530.

Singh, A.K., Sinha, O.P., Singh, R., 2023. Reduction behavior and kinetics of iron ore-charcoal composite pellets for sustainable ironmaking. Metall. Mater. Trans. B 54, 823–832. https://doi.org/10.1007/s11663-023-02729-0.

Sundberg, R. 2021. Reduction of iron oxides with hydrogen, Master Degree Thesis, Abo Akademy University.

Tang, K., Wang, Y.D., Niu, Y., Honeyands, T.A., O'Dea, D., Mostaghimi, P., Armstrong, R. T., Knackstedt, M., 2023. Particle classification of iron ore sinter green bed mixtures by 3D X-ray microcomputed tomography and machine learning. Powder Technol. 415, 118151 https://doi.org/10.1016/j.powtec.2022.118151.

Wei, W., Zheng, H., Runsheng, Xu., Fenglou, Wu., Chen, W., Jia, B., Xue, Z., 2019. Characterization of the mineral phases of the iron ore pellet via 3D reconstruction using serial sectioning. Metall. Res. Technol. 116, 117. https://doi.org/10.1051/metal/2018056.

Yazir, D., Sahin, B., Alkac, M., 2021. Selection of an inert gas system for the transportation of direct reduced iron. Mathem. Prob. Eng. 8529724. https://doi.org/10.1155/2021/8529724.

Yi, L., Huang, Z., Jiang, T., 2013. Sticking of iron ore pellets during reduction with hydrogen and carbon monoxide mixtures: Behavior and mechanism. Powder Technol. 235, 1001–1007. https://doi.org/10.1016/j.powtec.2012.11.043.

Zhang, S., Jiang, D., Wang, Z., Zong, Y., Zhang, J., Wang, F., Si, R., Zhang, S., Zhou, X., Pang, J., 2023. Sulfur migration behavior in sintering and pelletizing processes: A review. Steel Res. Int. https://doi.org/10.1002/srin.202200904.

Zhang, Z., Wong, J.J., Scott, S.A., Fennell, P.S., 2023. Spouted fluidised bed reactor for kinetic measurements of the reduction of Fe_2O_3 in a CO/CO_2 atmosphere part II: An extended random pore model for solid-state diffusion. Chem. Eng. Res. Des. 194, 597–609. https://doi.org/10.1016/j.cherd.2023.04.054.

Zheng, Z., Li, Y., Guo, Q., Zhang, L., Qi, T., 2023. Promoting the reduction reactivity of magnetite by introducing trace-K-ions in hydrogen direct reduction. Int. J. Hydrogen Energy 48 (48), 18177–18186. https://doi.org/10.1016/j.ijhydene.2023.01.268.